PROCEEDINGS OF SCIENCE

Measurement of the weak mixing phase ϕ_s through time-dependent CP violation in $B_s^0 \to J/\psi\phi$ decay in ATLAS

Tomáš Jakoubek*, **on behalf of the ATLAS collaboration**

Weizmann Institute of Science,
234 Herzl St., Rehovot 7610001, Israel

E-mail: tomas.jakoubek@cern.ch

An updated measurement of time-dependent CP asymmetry parameters in $B_s^0 \to J/\psi(\mu^+\mu^-)\phi(K^+K^-)$ decays using 80.5 fb^{-1} of integrated luminosity collected with the ATLAS detector during 2015-2017 from 13 TeV pp collisions at the LHC is presented. In the Standard Model, CP violation arises due to a single complex phase in the CKM quark mixing matrix. Precise measurements of the CKM parameters therefore constrain the Standard Model, and may reveal new physics effects. Results presented in this talk are compatible with those obtained from 19.2 fb^{-1} of 7 TeV and 8 TeV ATLAS data as well as with the Standard Model predictions and other LHC experiments. The measurement of the weak mixing phase ϕ_s improves on the precision of the previous ATLAS result by a factor of two.

40th International Conference on High Energy physics - ICHEP2020
July 28 - August 6, 2020
Prague, Czech Republic (virtual meeting)

*Speaker

PoS(ICHEP2020)387

1. Introduction

The $B_s^0 \to J/\psi\phi$ decay channel is expected to be sensitive to New Physics (NP) contributions to the CP violation. The source of the CP violation in this channel is an interference between direct decays and decays occurring through $B_s^0 - \overline{B_s^0}$ mixing. The interference is described by the weak phase difference ϕ_s between the $B_s^0 - \overline{B_s^0}$ mixing amplitude and the $b \to ccs$ decay amplitude. In the Standard Model (SM), the phase ϕ_s is related to CKM quark mixing matrix via the relation

$$\phi_s \simeq -2 \arg\left(-\frac{V_{ts}V_{tb}^*}{V_{cs}V_{cb}^*}\right).$$

Other parameters to describe the CP violation are the average decay width $\Gamma_s = (\Gamma_L^s + \Gamma_H^s)/2$, and the width difference $\Delta\Gamma_s = \Gamma_L^s - \Gamma_H^s$, where Γ_L^s and Γ_H^s are decay widths of the light (B_L) and heavy (B_H) mass eigenstates, respectively.

In case of no beyond the SM physics contributions to the B_s^0 mixing and decays, a value of $\phi_s = -0.03696^{+0.00072}_{-0.00082}$ rad is predicted [1]. Any significant deviation from this value is thus a clear sign of NP. Other parameters are not so sensitive to the NP since many models allow a larger value of ϕ_s whilst satisfying all other existing constraints.

An updated measurement of parameters describing the CP violation in the $B_s^0 \to J/\psi\phi$ decay using 80.5 fb^{-1} of LHC [2] pp collision data at $\sqrt{s} = 13$ TeV collected by the ATLAS [3] detector during 2015 - 2017 [4] is presented. The results are combined with those obtained from the analysis of 19.2 fb^{-1} of data collected at 7 TeV and 8 TeV [5].

2. The ATLAS detector

The ATLAS experiment is a multi-purpose particle detector at the LHC. The detector has a forward-backward symmetrical cylindrical geometry with almost 4π coverage. The inner-most part, the Inner Detector (ID), is used for a precise tracking. The ID subsystem covers the pseudorapidity region of $|\eta| < 2.5$ and is immersed in a 2 T axial magnetic field. A new Insertable B-Layer (IBL) [6, 7] was added to the present ID during the Long Shutdown 1. This layer with a radius of 33 mm was placed between a new beam pipe and the current inner pixel layer (B-layer). Due to this upgrade a more precise measurement of b-hadron decay time is possible. Electromagnetic and hadronic calorimeters and a Muon Spectrometer (MS) are located in between the solenoid providing the magnetic field for ID and three large superconducting air-core toroid systems. MS covers the pseudorapidity in the interval of $|\eta| < 2.7$.

3. Data reconstruction, candidate selection, and flavour tagging

The data were collected using several triggers based on the identification of a $J/\psi \to \mu\mu$ decay [8]. The transverse momentum (p_{T}) thresholds of these triggers are either 4 GeV or 6 GeV for the muons. To pass the selection, an event must contain at least one reconstructed primary vertex, formed from at least four ID tracks, and also at least one pair of oppositely charged muons reconstructed using information from both the MS and the ID.

Pairs of oppositely charged muon tracks are refitted to a common vertex and accepted if $\chi^2/\text{ndf} < 10$. To account for the varying mass resolution in different parts of the detector, the $|\eta(\mu)|$-dependent J/ψ mass cuts are applied. Candidates of $\phi \to K^+K^-$ are reconstructed from all pairs of oppositely charged tracks with $p_\text{T} > 1$ GeV and $|\eta| < 2.5$ that are not identified as muons.

B_s^0 candidates are further selected by fitting the four tracks to a common vertex with J/ψ mass constrain [9]. A candidate is accepted if the vertex fit has $\chi^2/\text{ndf} < 3$, a $\phi \to K^+K^-$ candidate satisfies $|m(K^+K^-) - m_\text{PDG}(\phi)| < 11$ MeV, and the B_s^0 candidate mass is in a range of $5.15\,\text{GeV} < m(B_s^0) < 5.65\,\text{GeV}$. If there is more than one B_s^0 candidate in the event, the one with the lowest χ^2/ndf is selected. In total 2 977 526 B_s^0 candidates pass the selection. For each candidate the proper decay time t is calculated as

$$t = \frac{L_{xy}\, m(B_s^0)}{p_\text{T}(B_s^0)},$$

where $p_\text{T}(B_s^0)$ denotes the reconstructed transverse momentum of the B_s^0 candidate and $m(B_s^0)$ is the mass of the B_s^0 meson taken from [9]. The transverse decay length L_{xy} is the displacement in the transverse plane of the B_s^0 meson decay vertex with respect to the primary vertex, projected onto the direction of the B_s^0 transverse momentum.

The initial flavour of the B_s^0 candidate is extracted using information from the semileptonic decay of the other B meson typically produced in the event. The flavour-sensitive discriminating variable is the *cone charge*, defined as a p_T-weighted sum of charge of tracks in the cone $\Delta R = \sqrt{(\Delta\phi)^2 + (\Delta\eta)^2} < 0.5$ around the leading lepton, i.e.,

$$Q_x = \frac{\sum_i^{N\ \text{tracks}} q_i \cdot (p_{\text{T}i})^\kappa}{\sum_i^{N\ \text{tracks}} (p_{\text{T}i})^\kappa},$$

where $x = \{\mu, e\}$ refers to muon or electron, respectively. If no lepton is present in the event, an attempt to construct a track jet is made and similarly defined jet-charge Q_jet is used as the discriminating variable. The value of the parameter κ is optimized for each tagging method to maximize its performance, i.e., the *tagging power* as defined in [4].

The tagging methods are calibrated using the decay channel $B^\pm \to J/\psi K^\pm$, where the flavour of the B meson at production is provided by the kaon charge. A cone charge Q_x is then mapped to a probability $P(B|Q_x)$ that a B meson is produced in a state containing a $\bar{b}$-quark.

4. Fit results and the combination with previous measurements

Parameters characterising the decay are extracted using an unbinned maximum likelihood fit performed on all candidates passing the selection. The likelihood function is defined as a combination of the probability density functions describing the signal (including a non-resonant S-wave state) and the mis-reconstructed and combinatorial backgrounds. The reconstructed mass m and its uncertainty σ_m, measured proper decay time t and its uncertainty σ_t, the transverse momentum p_T, the tagging probability $P(B|Q_x)$, and the transversity angles $(\theta_\text{T}, \psi_\text{T}, \phi_\text{T})$ of each B_s^0 candidate are used in the fit on the per-candidate basis. Selected parameters of the fit results are given in Table 1. Fit projections of mass, decay time, and transversity angles between final state particles are shown in Figure 1 and 2, respectively.

The likelihood fit determines two solutions with well separated values for the two of the 9 physical parameters – the strong phases $\delta_\parallel$ and $\delta_\perp$ related to the CP-even and CP-odd amplitudes in the decay, respectively. Figure 3 shows results of the 2D log-likelihood scan in the $\delta_\parallel - \delta_\perp$ plane, where the two minima are represented by 2D contours. The difference between the two solutions is $-2\Delta\ln(L) = 0.03$, favouring (a) but without ruling out (b). The two-fold nature of the likelihood minima has only a minor effect on all the other variables [4].

Parameter	7 TeV and 8 TeV Data			13 TeV Data			Combined		
	Value	Stat.	Syst.	Value	Stat.	Syst.	Value	Stat.	Syst.
ϕ_s [rad]	−0.090	0.078	0.041	−0.081	0.041	0.020	−0.087	0.036	0.019
$\Delta\Gamma_s$ [ps^{-1}]	0.085	0.011	0.007	0.0607	0.0047	0.0022	0.0641	0.0043	0.0024
Γ_s [ps^{-1}]	0.675	0.003	0.003	0.6687	0.0015	0.0018	0.6697	0.0014	0.0015

Table 1: Fit results for the selected physical parameters with their statistical and systematic uncertainties for the 7 TeV and 8 TeV data measurement [5], 13 TeV data measurement, and for their combination [4].

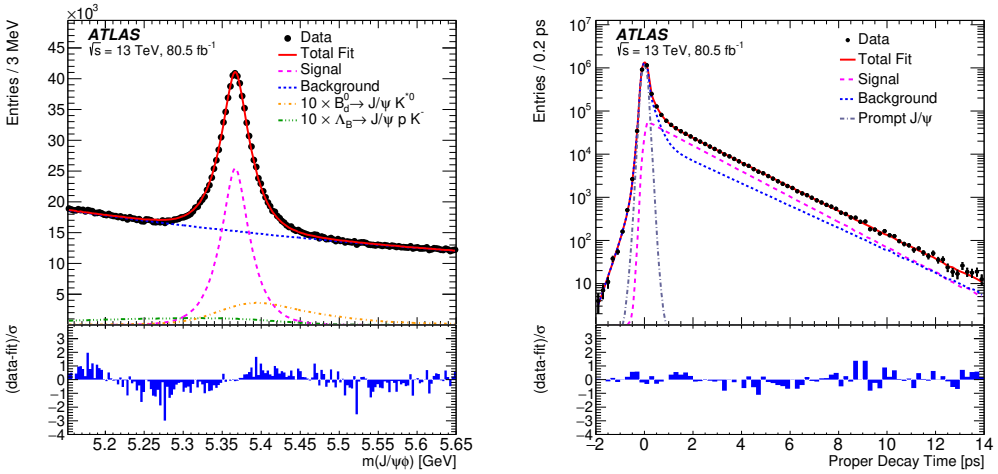

Figure 1: (Left) Mass fit projection for the $B_s^0 \to J/\psi\phi$ sample. The red line shows the total fit, the short-dashed magenta line shows the $B_s^0 \to J/\psi\phi$ signal component, the combinatorial background is shown as a blue dotted line, the orange dash-dotted line shows the $B_d^0 \to J/\psi K^{0*}$ component, and the green dash-dot-dot line shows the contribution from $\Lambda_b \to J/\psi pK^-$ events. (Right) Proper decay time fit projection for the $B_s^0 \to J/\psi\phi$ sample. The red line shows the total fit while the short-dashed magenta line shows the total signal. The total background is shown as a blue dotted line, and a long-dashed grey line shows the prompt J/ψ background component. Below each figure is a ratio plot that shows the difference between each data point and the total fit line divided by the statistical and systematic uncertainties summed in quadrature (σ) of that point [4].

Systematic uncertainties are evaluated for effects that are not accounted for in the likelihood fit. Flavour tagging, angular acceptance method, ID alignment, fit model used, trigger efficiency, mis-reconstructed background contributions, and limitation of the data modelling are identified as the main sources of systematic uncertainties, as described in detail in [4]. For each parameter, the total systematic uncertainty is obtained by adding these contributions in quadrature.

The fit results are compatible with those obtained from 19.2 fb^{-1} of 7 TeV and 8 TeV data analysis. A Best Linear Unbiased Estimator (BLUE) method [10, 11] is used to perform a combination of these measurements. The combined values for the selected parameters are also given in Table 1.

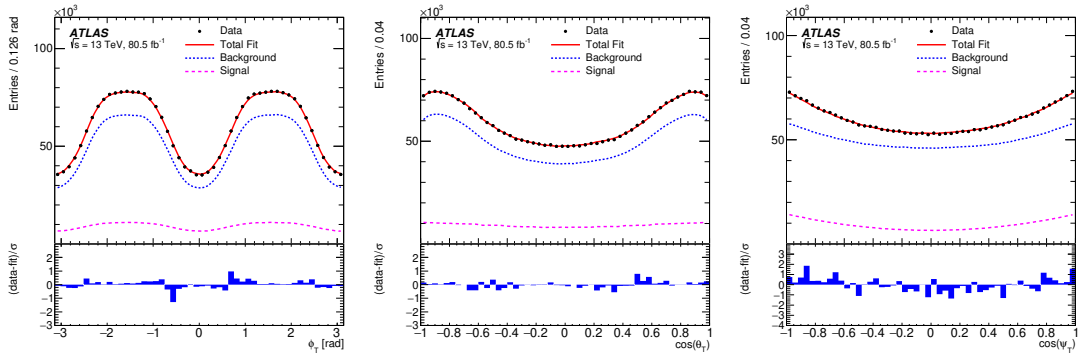

Figure 2: Fit projections for the transversity angles ϕ_{T} (left), $\cos(\theta_{\mathrm{T}})$ (middle), and $\cos(\psi_{\mathrm{T}})$ (right). In the plot the red solid line shows the total fit, the $B_s^0 \to J/\psi\phi$ signal component is shown by the magenta dashed line and the blue dotted line shows the contribution of all background components. Below the figure is a ratio plot that shows the difference between each data point and the total fit line divided by the statistical and systematic uncertainties summed in quadrature (σ) of that point [4].

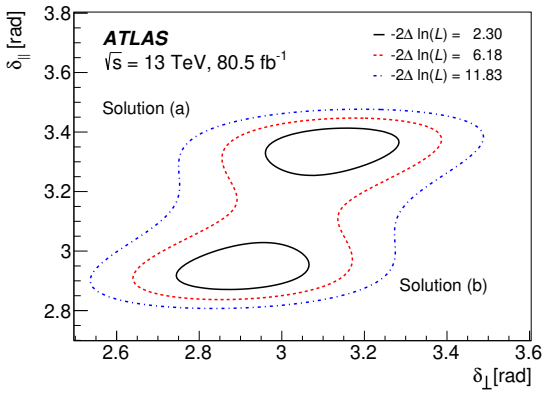

Figure 3: Two-dimensional constraints on the values of $\delta_{\parallel}$ and $\delta_{\perp}$ for solutions (a) and (b) at the level of $-2\Delta\ln(L) = 2.30$, 6.18, and 11.83, respectively, created using a full 2D scan. The minimum of the solution (b) is $-2\Delta\ln(L) = 0.03$ higher than the minimum of the solution (a) [4].

Figure 4 (left) shows two dimensional likelihood contours in the $\phi_s - \Delta\Gamma_s$ plane for the both ATLAS measurements and the combined result as well. The comparison of the results from ATLAS, CMS, and LHCb is shown on Figure 4 (right).

5. Summary

The updated analysis of the time-dependent CP asymmetry parameters in $B_s^0 \to J/\psi\phi$ decay using 80.5 fb^{-1} of integrated luminosity collected with the ATLAS detector from 13 TeV pp collisions at the LHC is presented. The results are compatible with those obtained from 19.2 fb^{-1} of 7 TeV and 8 TeV data and both measurements are statistically combined to the following results:

$$\begin{aligned} \phi_s &= -0.087 \pm 0.036(\text{stat.}) \pm 0.019(\text{syst.}) \text{ rad} \\ \Delta\Gamma_s &= 0.0641 \pm 0.0043(\text{stat.}) \pm 0.0024(\text{syst.}) \text{ ps}^{-1} \\ \Gamma_s &= 0.6697 \pm 0.0014(\text{stat.}) \pm 0.0015(\text{syst.}) \text{ ps}^{-1} \end{aligned}$$

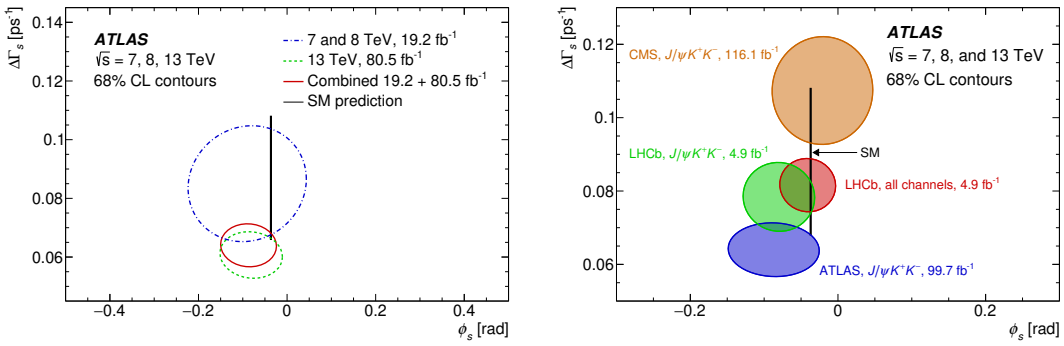

Figure 4: (Left) Contours of 68% confidence level in the $\phi_s - \Delta\Gamma_s$ plane, showing ATLAS results for 7 TeV and 8 TeV data (blue dashed-dotted curve), for 13 TeV data (green dashed curve) and for 13 TeV data combined with 7 TeV and 8 TeV (red solid curve) data. (Right) Contours of 68% confidence level in the $\phi_s - \Delta\Gamma_s$ plane, including results from CMS (orange) and LHCb (green) using the $B_s^0 \to J/\psi K^+K^-$ decay only and LHCb (red) for all the channels. The Standard Model prediction [1, 12] is shown as a very thin black rectangle. In all contours the statistical and systematic uncertainties are combined in quadrature and correlations are taken into account [4].

As can be seen on Figure 4 (left) and in Table 1, the precision of the CP-violating phase ϕ_s was improved by a factor of two. The updated measurement as well as the combination with the previous results is still consistent with the Standard Model predictions and with the other LHC measurements.

References

[1] J. Charles *et al.*, Phys. Rev. D **91** (2015) no.7, 073007, numbers updated using the results from the 2019 values in https://ckmfitter.in2p3.fr/www/results/plots_summer19/ckm_res_summer19.html.

[2] L. Evans and P. Bryant (editors), JINST **3** (2008), S08001.

[3] ATLAS Collaboration, JINST **3** (2008) S08003.

[4] ATLAS Collaboration, arXiv:2001.07115 [hep-ex].

[5] ATLAS Collaboration, JHEP **1608** (2016) 147.

[6] ATLAS Collaboration, CERN-LHCC-2010-013, CERN-LHCC-2012-009 (addendum).

[7] ATLAS IBL Collaboration, JINST **13** (2018) no.05, T05008

[8] ATLAS Collaboration, JINST **15** (2020) no.09, P09015.

[9] M. Tanabashi et al., Phys. Rev. D **98** (3 2018) 030001.

[10] L. Lyons, D. Gibaut and P. Clifford, Nucl. Instrum. Meth. A **270** (1988), 110.

[11] A. Valassi, Nucl. Instrum. Meth. A **500** (2003), 391-405.

[12] A. Lenz and U. Nierste, arXiv:1102.4274 [hep-ph].